RESEARCH ARTICLE | JANUARY 17 2017

Synthesis and characterization of boron doped diamond/β-SiC composite films

Haiyuan Fu; Hao Zhuang; Liang Yang; Thomas Hantschel; Song Ma; Zhidong Zhang; Xin Jiang

Appl. Phys. Lett. 110, 031601 (2017)
https://doi.org/10.1063/1.4974295

Synthesis and characterization of boron doped diamond/β-SiC composite films

Haiyuan Fu,[1] Hao Zhuang,[1] Liang Yang,[2] Thomas Hantschel,[3] Song Ma,[2] Zhidong Zhang,[2] and Xin Jiang[1,a)]
[1]*Institute of Materials Engineering, University of Siegen, Paul-Bonatz-Str. 9-11, 57076 Siegen, Germany*
[2]*Shenyang National Laboratory for Materials Science, Institute of Metal Research, Chinese Academy of Sciences, Shenyang 110016, China*
[3]*Imec, Kapeldreef 75, 3001 Leuven, Belgium*

(Received 4 October 2016; accepted 6 January 2017; published online 17 January 2017)

Boron doped diamond/β-SiC composite films with a conductive diamond phase separated by the insulating β-SiC phase are fabricated by the microwave plasma chemical vapor deposition process. By manipulating the gas phase composition during the film deposition, the boron incorporation and diamond/β-SiC ratio in the composite film are well controlled. Scanning electron microscopy, transmission electron microscopy, Raman and X-ray diffraction measurements are carried out to study the structural composition of the films. It is observed that the introduction of boron during the growth process does not affect the independent growth of diamond and β-SiC crystals with high crystal quality. Scanning spreading resistance microscopy measurements confirm the presence of the conductive diamond phase and the insulating β-SiC phase in the film. The observed differences in the conductivities between diamond and β-SiC are explained by the different boron acceptor levels in diamond and β-SiC crystals. Cyclic voltammetry measurements are carried out to study the electrochemical property of the films. Our results demonstrate that boron doped diamond/β-SiC composite films are a good candidate for electroanalysis applications whereby exploiting diamond's high chemical and dimensional stability as well as its excellent electrochemical properties. *Published by AIP Publishing.* [http://dx.doi.org/10.1063/1.4974295]

Composite electrodes, which consist of conductive regions separated by at least one insulating phase,[1–3] are of great interest to material scientists, physicists, and chemists due to the advantages they offer, i.e., high flexibility in the size and shape of the material, easy adaptation to a variety of electrode configurations; precious metal composite electrodes offer less weight and lower cost per unit compared to pure precious-metal electrodes, etc.[1] Nevertheless, the most attractive advantage is their higher signal-to-noise (S/N) ratio[1] over their pure conductor counterparts during electroanalysis, due to the presence of overlapping diffusion zones in their composite structure; and the high physical and chemical stability[4] of the electrodes. Such features along with the possibilities in the selective modification of the conductive and/or insulating phases (physically and/or chemically)[5,6] allows for many potential applications. Even though various materials have been applied to construct composite electrodes,[7–10] carbon based nanomaterials, i.e., carbon nanotubes, graphene, nanographite, etc., are the most popular candidates for the conductive phase.[11–16] As a well-known allotrope of carbon, diamond is famous for its extraordinary physical and chemical qualities.[17,18] However, no diamond based composite electrode has been fabricated and studied in detail until today. Considering the high chemical and dimensional stability of diamond as well as its wide electrochemical potential window and low background current,[19,20] diamond is believed to be a better alternative for the fabrication of composite electrodes. The main obstacle in the fabrication of diamond based composite electrodes lies in the lack of well-dispersed conductive diamond nanostructures,[21] which makes the conventional strategy applied for the fabrication of carbon-based composite electrode inapplicable in the case of diamond. The latter normally involves mixing the carbon nanostructures with insulating binders, i.e., ion liquid,[12] paraffin oils, sol-gel derived silica,[22] epoxy,[23] etc.

An alternative approach for the fabrication of a diamond-based composite electrode is the direct "bottom-up growth" of the material. Although chemical vapor deposition (CVD) diamond synthesis involves extreme growth conditions, several carbides can still co-grow with diamond to form composite films.[24–26] Among them, diamond/β-SiC composite films have been systematically investigated since 1992.[26] In this composite system, the crystallinity, ratio, and phase distribution of both diamond and β-SiC can be well controlled by manipulating the synthetic parameters.[27–29] It is well known that diamond can be doped with boron, which forms a shallow acceptor level in diamond. Depending on the boron concentration, the conductivity of diamond can be altered from semi-conductive to metallically conductive. In contrast, the boron forms only a deep acceptor level (ionization energy: 0.735 V) in β-SiC, even though it has a high solubility in β-SiC.[30] This leads to a negligible ionization of the boron impurity in β-SiC at room temperature, despite of the high concentration of uncompensated acceptors. Inspired by the facts mentioned above, we demonstrate in the present study the one-step fabrication of the diamond-based composite electrode through *in-situ* boron doping of the diamond/β-SiC composite film. Consequently, we show that a diamond/

a)Author to whom correspondence should be addressed. Electronic mail: xin.jiang@uni-siegen.de. Tel.: +49 271 740 2966. Fax: +49 271 740 2442.

β-SiC composite film with the conductive diamond phase separated by the insulating β-SiC phase is obtained.

Single-crystalline Si (100) wafers (resistivity $>10\,000\,\Omega$ cm) were used as substrates for the deposition of the composite thin films. The Si wafers were pretreated for 30 min in a suspension containing 0.05 wt. % nanodiamond particles (5 nm in size, New Metals & Chemicals Corporation, Japan) in order to achieve a high diamond nucleation density. The deposition was carried out at a constant gas pressure of 45 Torr and a substrate temperature of $\sim$700 °C, which was measured by an optical pyrometer; a microwave power of 1800 W was used to sustain the plasma. The reactive gas featured a mixture of H_2, CH_4, $Si(CH_3)_4$ [tetramethylsilane (TMS)] and $B(CH_3)_3$ [trimethylboron (TMB)]. H_2 served as a precursor, CH_4 was for the diamond growth and TMS for the SiC growth; TMB was added as a boron source for doping. For all the films discussed here, the total gas flow rate was maintained at 400 sccm (cubic centimeter per minute at STP), and the CH_4 concentration was kept at 1%. TMS gas additions varied in different experiments from 0 to 0.043% and the TMB concentration varied from 0 to 170 ppm. The deposition was carried out for 6 h and the thickness of the films was 1 μm. Scanning electron microscopy (SEM, Zeiss Ultra 55) and transmission electron microscopy (TEM, Tecnai G2 F30) inspections were carried out to obtain the structural information of the samples. X-ray diffraction (XRD) measurements were performed by an XRD 3000 PTS diffractometer (GE Inspection Technologies GmbH) in the 2θ range of 34°–100° with a step size of 0.05°. The Joint Committee on Powder Diffraction Standards cards (JCPDS cards-card No. 65-0537 for diamond and card No. 29-1129 for β-SiC) were used for indexing the observed diffraction peaks. The spectra in the 2θ range of 65°–75° were excluded due to the strong Si (400) diffraction peak. Micro Raman scattering studies were carried out on a self-constructed Raman spectrometer to understand the structural order and boron incorporation into diamond. The 532 nm line of a Nd:YVO_4 diode-pumped solid-state laser was used as the excitation source. A liquid nitrogen cooled back illuminated the charge-coupled device (CCD) camera (Symphony CCD, HORIBA Jobin Yvon) with single photon sensitivity that was used for spectrum detection. The resistivity of the films was measured by the four-point-probe technique with a PPMS system (Quantum Design) within the temperature range from 1.9 K to 400 K, cooled by liquid He. A Bruker Dimension Icon PT atomic force microscopy (AFM) system equipped with a scanning spreading resistance microscopy (SSRM)[31] application module using a DC bias of +0.5 V was applied to obtain the surface topographical (AFM) and electrical (SSRM) information. Electrochemical measurements were carried out by a potentiostat (CHI 660E) with a three-electrode configuration: the fabricated thin films were used as the working electrode, a platinum wire was used as the counter electrode, and Ag/AgCl (3 M KCl) was used as the reference electrode.

Figure 1 shows the room temperature electrical conductivities of the films deposited with different TMB additions, to control the boron incorporation, while keeping the other parameters constant. It is clearly observable that all the films are electrically conductive, indicating the active boron doping of the films. The conductivity is dependent on the TMB addition: with increasing boron concentration from 30 ppm to 170 ppm, the conductivity σ increases significantly from 5 to 100 S/cm. When the boron concentration increases from 30 ppm to 90 ppm, the conductivity σ increases from 5 S/cm to 15 S/cm slowly; with further increasing TMB addition, a slightly larger slope is observed in the diagram, resulting in a high conductivity for a semi-conductor material. This is not surprising, as it is well known that both diamond and β-SiC crystals can be doped with boron. With increasing boron incorporation, the conductivity of the films is expected to increase. Especially in the case of diamond, boron forms a shallow acceptor level in diamond. With increasing boron incorporation, near metallic conductivity of diamond is achieved while it keeps its superior diamond characteristics.

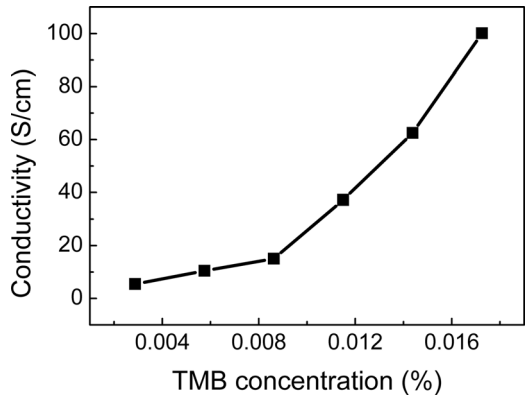

FIG. 1. Electrical conductivity at room temperature of the diamond/β-SiC composite films deposited at different TMB concentrations ranging from 30 to 170 ppm. The methane and TMS concentrations are kept at 1 and 0.043%, respectively.

Figures 2(a)–2(c) shows the SEM surface morphology of the composite films deposited with different TMB additions while keeping the CH_4 and TMS concentrations at 1% and 0.043%, respectively. Note that the bright and dark regions in the SEM image are corresponding to the diamond and β-SiC areas,[32] respectively, which is further confirmed by the different phase contrasts in the backscattered electron images (BSE) in Figures 2(a)–2(c). Micrometer-sized diamond ($\sim$1 μm) and β-SiC (0.2–0.5 μm) grains are clearly observable in all the films, indicating the high crystal quality of both diamond and β-SiC. The crystal size and the overall morphology of diamond and β-SiC remains nearly unchanged with increasing TMB concentration. Such an observation is different from one of our previous studies, in which a low microwave power is applied, and the introduction of TMB leads to the formation of (001)-oriented diamond crystals.[33] In the present study, the unchanged crystal quality of diamond and β-SiC is attributed to the usage of a high microwave power. At a high microwave power, the concentration of atomic hydrogen is drastically increased, which significantly suppresses the formation of crystal defects during the growth of diamond and β-SiC crystals, leading to the selective growth of diamond and β-SiC crystals with high crystal quality in the film.[29] For a better understanding of the structure of the fabricated boron doped diamond/β-SiC composite films, transmission electron microscopy (TEM) images are shown in the supplementary material in Figure S1.

Figure 2(d) depicts the XRD patterns of the above films. All the peaks can be indexed to diamond and β-SiC,

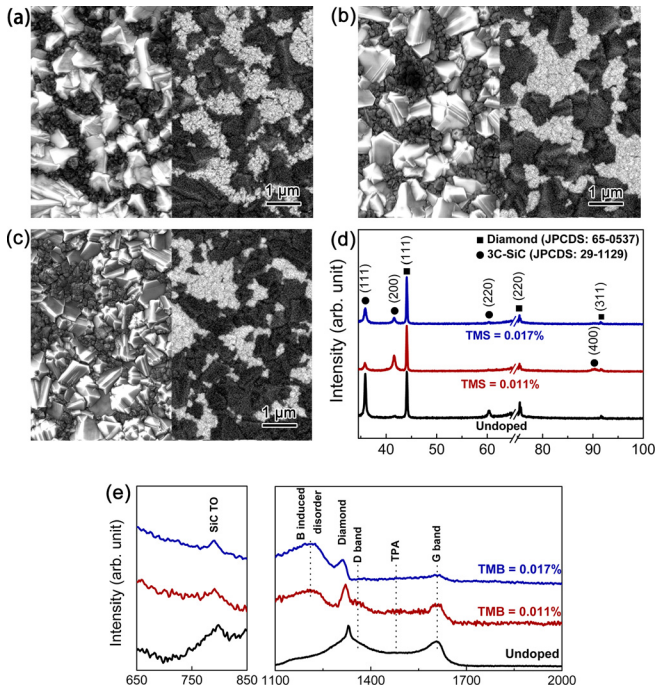

FIG. 2. (a)–(c) SEM images (left—secondary electron mode, right—backscattered electron mode) of the diamond/β-SiC composite films deposited at different TMB concentration while keeping the methane and TMS concentrations constant at 1% and 0.043%, respectively. (a) TMB = 0, (b) TMB = 0.011%, (c) TMB = 0.017%. (d) XRD and (e) Raman spectra of the above films.

confirming that all the films are composed of diamond and β-SiC phases. No preferential orientation is observable indicating the randomly oriented polycrystalline nature of both diamond and β-SiC phases in all the films. However, a slight variation in the intensity of the peaks corresponding to β-SiC still exists: the intensity of the peak corresponding to the (111) β-SiC reflex drastically decreases for the samples deposited with TMB addition, indicating a slightly increased (001) orientation of the β-SiC phase when TMB is involved. The latter is supported by the presence of stronger (002) and (004) peaks in the XRD spectra. Figure 2(e) depicts the corresponding Raman spectra of the above films. For all the films considered, the SiC transverse optical (TO) peak positioned at 800 cm^{-1} is observable, confirming the existence of the β-SiC phase with high crystallinity in the films. For the undoped composite film, a sharp diamond Raman peak positioning at 1332 cm^{-1} (first-order diamond Raman band) as well as the peaks corresponding to the D and G band related to the existence of amorphous carbon at the grain boundaries are clearly observable. When 0.011 ppm of TMB is introduced, the characteristic diamond Raman peak shifts to lower wave numbers because of the "Fano" effect, indicating the doping of diamond with boron.[34] Another peak located at ~1200 cm^{-1} can be seen as well, which is attributed to the boron-induced distortion of the diamond lattice.[34] With increasing boron concentration to 170 ppm, the diamond Raman peak further shifts to lower wave numbers and the intensity of the 1200 cm^{-1} peak becomes higher, indicating the increased boron incorporation in the diamond crystals.[34] In addition to the change in the diamond related Raman peaks, the SiC TO peak also shifts to lower wave numbers. This is due to the occupation of Si by boron in the SiC lattice.[35,36] The formed B-C bond is shorter than the Si-C bond, which leads to a released biaxial tensile stress and decreases the phonon oscillation frequency,[35,36] indicating the doping of β-SiC with boron.

From the above observations, we confirm that boron is incorporated in the diamond and β-SiC crystals. Meanwhile, the introduction of TMB during the growth of the diamond/β-SiC composite film does not affect the formation and crystal quality of diamond and β-SiC phases under the present deposition conditions. We elucidate now the differences in the electrical conductivities of the diamond and β-SiC phases in the film. For this purpose, SSRM measurements[37] are carried out on the sample surface depicted in Figure 2(b) and the results are shown in Figures 3(a) and 3(b). As discussed in Figures 2(a)–2(c), the diamond and β-SiC crystals show significant differences in the crystal sizes: diamond crystals are larger than the β-SiC crystals. Such a feature enables us to distinguish the diamond and β-SiC in the SSRM topographical image. Two regions corresponding to β-SiC crystals are marked clearly with green lines in Figure 3(a). Figure 3(b) shows the corresponding electrical mapping of the same region, in which, the conductive regions are represented by a dark color and the non-conductive regions are represented by a bright color. Note the strong differences in the surface conductivities of about 5 orders of magnitudes between the two different distinguishable regions, with the conductive regions showing a measured resistance value of 10^6 Ω and the non-conductive regions showing a resistance of 10^{11} Ω. By comparing Figure 3(b) with Figure 3(a), it can be concluded that the conductive regions correspond to diamond and the non-conductive regions correspond to β-SiC. The differences in the conductivities of diamond and β-SiC originate from the different energy levels of the boron acceptor in diamond and β-SiC. Boron forms shallow acceptor levels in diamond depending on the boron incorporation.[38] As a result, a high room temperature conductivity of diamond can be achieved upon TMB addition. Nevertheless, boron only forms a deep acceptor level (0.735 V) in β-SiC. Even though the boron incorporation might be high in β-SiC, due to the large binding energy, the thermal energy at and below room temperature is not sufficiently high to generate a substantial amount of holes for conduction, on the other hand, the B-derived acceptor levels are believed to effectively trap the carriers,[39] leading to the poor room temperature conductivity of β-SiC in the present study. The results shown above strongly confirm the fabrication of the composite electrode from diamond in the present study. The electrochemical properties of the films were also characterized using cyclic voltammetry. Figure 3(c) shows the voltammograms of the boron doped diamond/β-SiC composite film and the pure boron doped diamond film at a scan rate of 100 mV/s in 0.1 M H_2SO_4. The capacitances (C, $\mu F/cm^2$) were calculated to be 4.3 $\mu F/cm^2$ and 5.13 $\mu F/cm^2$, respectively, for the composite film and the pure diamond electrode. The background current of the composite electrode is 20% lower than that of the pure diamond film. The background current is an important criterion for evaluating the electrode for sensor applications: the lower the background current is, the higher the signal to noise ratio of the sensor will be. Therefore, the low

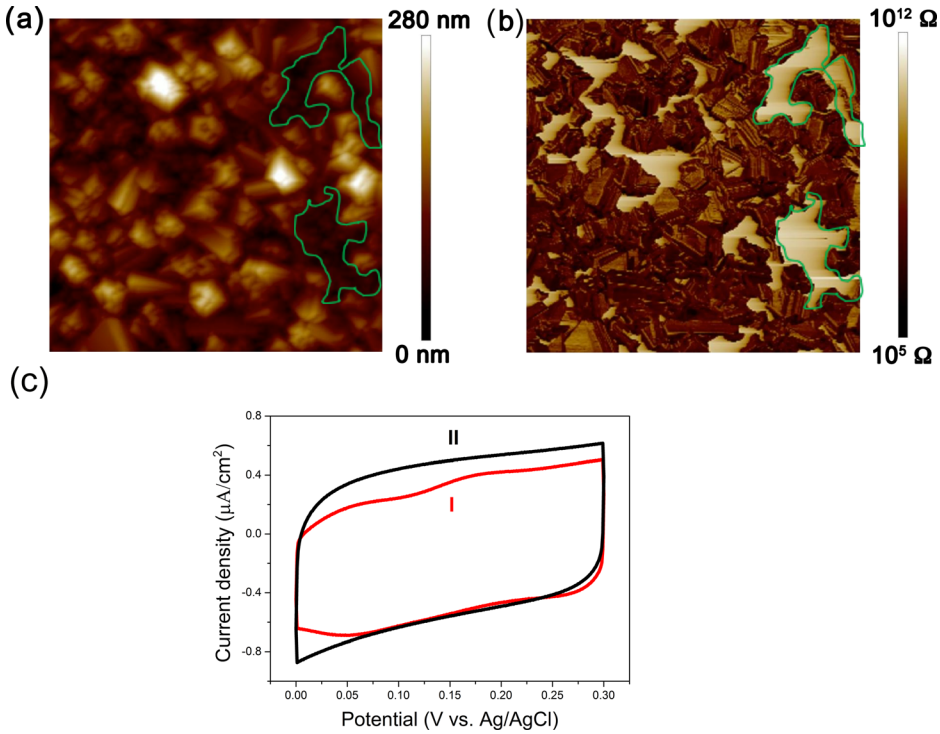

FIG. 3. (a) topographical map, (b) corresponding electrical map of SSRM measurements of $5 \times 5\,\mu m^2$ scan area of the surface of the boron doped diamond/β-SiC composite film deposited at TMB, TMS, and methane concentrations of 0.011%, 0.043%, and 1%, respectively; (c) cyclic voltammetry diagram of (I) boron doped diamond/β-SiC composite film and (II) pure boron doped diamond film at a scan rate of 100 mV/s in the solution of 0.1 M H_2SO_4.

background current of the composite electrode looks very promising for electrochemical sensor applications.

Another important feature in the fabrication of the composite electrode is to control the amount of the insulating and the conductive phases, so that the electrical properties as well as the performance of the electrode can be controlled. In the present study, we have been able to control the diamond/β-SiC ratios in the composite films by controlling the TMS concentration in the gas phase while keeping the other deposition parameters constant. Figures 4(a)–4(c) show the SEM surface images of the films deposited at different TMS concentrations. In an extreme case when the TMS concentration is zero, a pure boron doped diamond film is produced, as shown in Figure 4(a) which is well recognizable/characterized by no dark

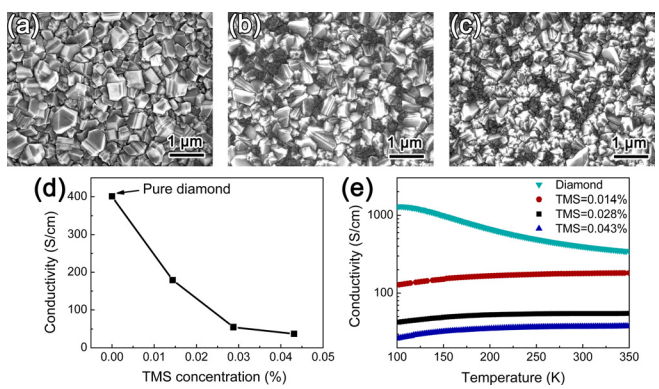

FIG. 4. (a)–(c) SEM images of the diamond/β-SiC composite films deposited at different TMS concentrations while keeping the methane and TMB concentration constant at 1% and 0.011%, respectively: (a) TMS = 0 (pure diamond film, for the purpose of comparison), (b) TMS = 0.014% and (c) TMS = 0.028%; (d) room temperature electrical conductivities and (e) temperature dependence of the electrical conductivities of the films deposited at different TMS concentrations.

β-SiC phases being observed in SEM in-lens mode imaging.[33] By increasing the TMS concentration from 0.014% (Figure 4(b)) to 0.028% (Figure 4(c)) and then further to 0.043% (Figure 2(b)), an increase in the amount of the β-SiC phase can be observed. This can be seen by the increasing number and area of the dark β-SiC phases competing with the bright diamond phases in the SEM images. The electrical conductivities of the films with different diamond/β-SiC ratios are shown in Figures 4(d) and 4(e). Obviously, with an increasing amount of the insulating β-SiC phase in the film, the electrical conductivities of the films significantly drop from 400 S/cm for pure diamond film to 38 S/cm for the film deposited with a TMS concentration of 0.043%. The temperature dependence of the film conductivity (Figure 4(e)) indicates that the pure diamond film is metallically doped in the present study: an increase in the temperature results in the decrease of the electrical conductivity. This is commonly observed in diamond films when the boron incorporation is high.[40] Nevertheless, the composite films all show a semiconductor behavior: an increase in the temperature results in an increase in the electrical conductivity. Such a phenomenon implies that the temperature dependence of the electrical conductivity of the composite film is dominated by the β-SiC phase in the film. With a much higher resistance than the diamond phase, the conductivity change of the β-SiC phase has a correspondingly higher impact on the film's behavior. When the temperature increases, the electrical conductivity of the insulating β-SiC phase increases as a semiconductor because of the thermal excitation, which in turn results in the increased macroscopic conductivity of these composite films (albeit at clearly lower conductivity levels compared to pure boron doped diamond films).

In conclusion, boron doped diamond/β-SiC composite films with a conductive diamond phase and an insulating β-SiC phase are fabricated in the microwave plasma chemical vapor deposition process. The boron incorporation and

diamond/β-SiC ratio in the composite films are controlled by manipulating the gas phase composition. SEM, TEM, Raman, and XRD measurements are carried out to study the structural information of the films. It is observed that the introduction of boron during the growth process does not influence the independent growth of diamond and β-SiC. SSRM measurements confirm that the diamond phase in the composite film is metallically conductive while the β-SiC phase is insulating. The electrochemical performance of the film was evaluated by cyclic voltammetry measurements, showing a lower background current for the composite film. This makes the composite film very promising for sensor applications. Future work will be carried out to explore the suitable structuring of those composite films by patterning of the composite film during growth as well as their further surface modification to create an optimal structure for electrochemical sensor applications.

See supplementary material for the TEM observations of the boron doped diamond/β-SiC composite films.

The authors would like to thank Deutsche Forschungsgemeinschaft (DFG JI 22/24-1) and the National Natural Science Foundation of China (Nos. 51271178, 51571195, and 51590883) for the financial support. Zheng Xu is acknowledged for carrying out the SSRM measurements. Siyu Yu is acknowledged for the help with cyclic voltammetry measurements. Bing Yang is acknowledged for the help with TEM measurements.

[1]D. E. Tallman and S. L. Petersen, Electroana **2**, 499 (1990).
[2]S. M. Aharoni, J. Appl. Phys. **43**, 2463 (1972).
[3]H. Zhao and D. O'Hare, J. Phys. Chem. C **112**, 9351 (2008).
[4]G. Gun, M. Tsionsky, and O. Lev, Anal. Chim. Acta **294**, 261 (1994).
[5]S. Sampath and O. Lev, Anal. Chem. **68**, 2015 (1996).
[6]J. Gun, M. Tsionsky, L. Rabinovich, Y. Golan, I. Rubinstein, and O. Lev, J. Electroanal. Chem. **395**, 57 (1995).
[7]J.-D. Kim, G.-D. Kim, J.-W. Moon, Y.-I. Park, W.-H. Lee, K. Kobayashi, M. Nagai, and C.-E. Kim, Solid State Ionics **143**, 379 (2001).
[8]X. M. Liu and X. G. Zhang, Electrochim. Acta **49**, 229 (2004).
[9]D. Ravi Shankaran, K. Iimura, and T. Kato, Sens. Actuators, B **94**, 73 (2003).
[10]J. Wang, J. Chen, K. Konstantinov, L. Zhao, S. H. Ng, G. X. Wang, Z. P. Guo, and H. K. Liu, Electrochim. Acta **51**, 4634 (2006).
[11]I. Corb, F. Manea, C. Radovan, A. Pop, G. Burtica, P. Malchev, S. Picken, and J. Schoonman, Sensors **7**, 2626 (2007).
[12]N. Maleki, A. Safavi, and F. Tajabadi, Anal. Chem. **78**, 3820 (2006).
[13]B. Serra, S. Jiménez, M. L. Mena, A. J. Reviejo, and J. M. Pingarrón, Biosens. Bioelectron. **17**, 217 (2002).
[14]H. Zhang, G. Cao, Z. Wang, Y. Yang, Z. Shi, and Z. Gu, Electrochem. Commun. **10**, 1056 (2008).
[15]J. H. Park, J. M. Ko, O. O. Park, and D.-W. Kim, J. Power Sources **105**, 20 (2002).
[16]S. Palanisamy, S. Cheemalapati, and S.-M. Chen, Anal. Biochem. **429**, 108 (2012).
[17]*Thin Film Diamond: I*, edited by C. E. Nebel and W. Ristein (Elsevier, Amsterdam, 2003).
[18]*Thin Film Diamond: II*, edited by C. E. Nebel and W. Ristein (Elsevier, Amsterdam, 2004).
[19]A. Fujishima, Y. Einaga, T. N. Rao, and D. A. Tryk, *Diamond Electrochemistry* (Elsevier B.V., Amsterdam, 2005).
[20]N. Yang, J. S. Foord, and X. Jiang, Carbon **99**, 90 (2016).
[21]S. Heyer, W. Janssen, S. Turner, Y.-G. Lu, W. S. Yeap, J. Verbeeck, K. Haenen, and A. Krueger, ACS Nano **8**, 5757 (2014).
[22]M. Tsionsky, G. Gun, V. Glezer, and O. Lev, Anal. Chem. **66**, 1747 (1994).
[23]M. Pumera, A. Merkoçi, and S. Alegret, Sens. Actuators, B **113**, 617 (2006).
[24]F. Ding and Y. Shi, Surf. Coat. Technol. **201**, 5050 (2007).
[25]H. A. Samra, R. Hong, and X. Jiang, Chem. Vap. Deposition **13**, 17 (2007).
[26]X. Jiang and C. P. Klages, Appl. Phys. Lett. **61**, 1629 (1992).
[27]X. Jiang and C. P. Klages, Diamond Relat. Mater. **2**, 523 (1993).
[28]Y. L. Shi, M. H. Tan, and X. Jiang, J. Mater. Res. **17**, 1241 (2002).
[29]H. Zhuang, L. Zhang, T. Staedler, and X. Jiang, Scr. Mater. **65**, 548 (2011).
[30]H. Kuwabara and S. Yamada, Phys. Status Solidi A **30**, 739 (1975).
[31]P. De Wolf, J. Snauwaert, T. Clarysse, W. Vandervorst, and L. Hellemans, Appl. Phys. Lett. **66**, 1530 (1995).
[32]H. Zhuang and X. Jiang, Surf. Coat. Technol. **249**, 84 (2014).
[33]H. Zhuang, H. Fu, and X. Jiang, Surf. Coat. Technol. **259**, 526 (2014).
[34]S. Prawer and R. J. Nemanich, Philos. Trans. R. Soc., A **362**, 2537 (2004).
[35]Y. Ou, V. Jokubavicius, S. Kamiyama, C. Liu, R. W. Berg, M. Linnarsson, R. Yakimova, M. Syväjärvi, and H. Ou, Opt. Mater. Express **1**, 1439 (2011).
[36]X.-B. Li, Z.-Z. Chen, and E.-W. Shi, Physica B **405**, 2423 (2010).
[37]M. Tsigkourakos, T. Hantschel, C. Bangerter, and W. Vandervorst, Phys. Status Solidi A **211**, 2284 (2014).
[38]T. Klaus, Semicond. Sci. Technol. **18**, S20 (2003).
[39]K. J. Kim, K. Y. Lim, Y. W. Kim, and H. C. Kim, J. Am. Ceram. Soc. **96**, 2525 (2013).
[40]T. Yokoya, T. Nakamura, T. Matsushita, T. Muro, Y. Takano, M. Nagao, T. Takenouchi, H. Kawarada, and T. Oguchi, Nature **438**, 647 (2005).